

DIFFERENTIAL ROTATION IN NEUTRON STARS: MAGNETIC BRAKING AND VISCOUS DAMPING

STUART L. SHAPIRO¹

Department of Physics, University of Illinois at Urbana-Champaign, Urbana, IL 61801

ABSTRACT

Differentially rotating stars can support significantly more mass in equilibrium than nonrotating or uniformly rotating stars, according to general relativity. The remnant of a binary neutron star merger may give rise to such a “hypermassive” object. While such a star may be dynamically stable against gravitational collapse and bar formation, the radial stabilization due to differential rotation is likely to be temporary. Magnetic braking and viscosity combine to drive the star to uniform rotation, even if the seed magnetic field and the viscosity are small. This process inevitably leads to delayed collapse, which will be accompanied by a delayed gravitational wave burst and, possibly, a gamma-ray burst. We provide a simple, Newtonian, MHD calculation of the braking of differential rotation by magnetic fields and viscosity. The star is idealized as a differentially rotating, infinite cylinder consisting of a homogeneous, incompressible conducting gas. We solve analytically the simplest case in which the gas has no viscosity and the star resides in an exterior vacuum. We treat numerically cases in which the gas has internal viscosity and the star is embedded in an exterior, low-density, conducting medium. Our evolution calculations are presented to stimulate more realistic MHD simulations in full 3+1 general relativity. They serve to identify some of the key physical and numerical parameters, scaling behavior and competing timescales that characterize this important process.

1. INTRODUCTION

Neutron stars may form with appreciable differential rotation. The merger of a binary neutron star system, for example, will form a differentially rotating remnant, an outcome considerably enhanced by the likelihood that the neutron stars are nearly irrotational before coalescence (Bildsten and Cutler 1992; Kochanek 1992; Lai, Rasio & Shapiro 1993). The formation of a differentially rotating remnant following binary merger was first demonstrated in Newtonian hydrodynamic simulations (see e.g., Rasio and Shapiro 1992,1994,1999) and dramatically confirmed in fully relativistic simulations (Shibata & Uryu 2000), where the remnant’s core is found to rotate appreciably faster than its envelope. Core collapse in a supernova may also result in a differentially rotating neutron star, even if the rotation of the progenitor at the onset of collapse is only moderately rapid and almost uniform (see, eg, Zwerger & Müller 1997; Rampp, Müller & Ruffert 1998, and references therein). Conservation of angular momentum during collapse causes the ratio $\beta = T/|W|$, where T is the rotational kinetic energy and W is the gravitational potential energy, to grow like R^{-1} , where R is the equatorial radius. Thus β can increase by several orders of magnitude during the implosion. Since uniformly rotating, compressible stars can only support very small values of β in equilibrium without shedding mass at the equator (see, e.g., Tassoul 1978, Shapiro & Teukolsky 1983), collapsed cores of rapidly rotating progenitors must acquire some degree of differential rotation at birth as they settle into equilibrium. Similar arguments hold for accretion-induced collapse of white dwarfs to neutron stars.

Differentially rotating neutron stars can support significantly more rest mass than their nonrotating or uniformly rotating counterparts. Baumgarte, Shapiro & Shibata (2000; hereafter BSS), have recently constructed relativistic equilibrium models of differentially rotating “hypermassive” polytropes. These configurations have rest masses that exceed both the maximum

rest mass of nonrotating spherical stars (the TOV limit) and uniformly rotating stars at the mass-shedding limit (“supramassive stars”), all with the same polytropic index. BSS performed dynamical simulations in full general relativity to demonstrate that hypermassive stars can be constructed that are dynamically stable against radial collapse and nonradial bar formation (see also Shibata, Baumgarte & Shapiro 2000). The fully relativistic binary coalescence calculation of Shibata & Uryu (2000) reveals that such a dynamically stable hypermassive star can arise following binary merger. BSS have argued that the dynamical stabilization of a hypermassive remnant by differential rotation may lead to delayed collapse and a delayed gravitational wave burst. The reason is that the stabilization due to differential rotation, although expected to last for many dynamical timescales (i.e. many milliseconds), will ultimately be destroyed by magnetic braking and/or viscosity. These processes drive the star to uniform rotation, which cannot support the excess mass, and will lead to catastrophic collapse, possibly accompanied by some mass loss.

The purpose of this paper is to provide a time-dependent calculation of the damping of differential rotation by magnetic braking and viscosity in a rapidly spinning star. The goal is to construct an exact, albeit idealized, Newtonian model which readily reveals some of the important physical effects, together with their timescales and scaling behavior. By adopting a sufficiently simple, laminar model with a high degree of spatial symmetry, we are able to perform a tractable analysis of the evolution from first principles and without approximation. Our motivation for this simplified approach is to help identify the minimum ingredients for a more realistic, future numerical calculation in full general relativity. We wish to demonstrate explicitly why it is essential to include magnetic fields in fully relativistic simulations of the late stages of coalescing binary neutron stars and other dynamical scenarios where differential rotation naturally arises and significantly influences the struc-

¹Department of Astronomy and NCSA, University of Illinois at Urbana-Champaign, Urbana, IL 61801

ture and stability of the final configuration. The results have important implications for the detection of gravitational wave and gamma-ray bursts (BSS; Spruit 1999a).

Our discussion is by no means the first, (see, e.g., Spitzer 1978 for discussion and references on magnetic braking of angular momentum in interstellar clouds; see Spruit (1999b) and references therein for a discussion of differential rotation and the evolution of initially weak magnetic fields in stellar interiors), and surely will not be the last on this nontrivial topic, especially given the simplified nature of our model. However, the importance of magnetic braking has been pointed out only recently in the context of binary neutron star coalescence, differential rotation of the remnant and the emission of gravitational waves following delayed collapse (BSS). Presumably the most effective way to stimulate numerical relativists to include magnetic fields in 3+1 fully relativistic hydrodynamics codes now under development is to provide a concrete calculation demonstrating their physical importance, which we do below.

In Section 2 we describe our basic model. In Section 3 we set out the fundamental equations and put them in a convenient nondimensional form. In Section 4 we summarize solutions for three distinct cases, depending on whether the stellar exterior region is a pure vacuum or filled with conducting plasma, and whether or not we include viscosity. In the first case (vacuum exterior, no viscosity) our treatment is entirely analytic, while in the other two the analyses are numerical. In Section 5 we restore dimensions and evaluate our key results for the case of a differentially rotating remnant of a binary neutron star merger. Here we summarize the implications of our calculations to future observations and numerical simulations. Appendices A and C summarize details of our numerical calculation, while Appendix B provides a proof that the lowest energy state for our adopted rotating stellar models is the state of uniform rotation, for fixed angular momentum.

2. BASIC MODEL

As discussed in BSS, differential rotation in a spinning star twists up a frozen-in, poloidal magnetic field, creating a very strong toroidal field. This process will generate Alfvén waves, which can redistribute and even carry off angular momentum from a star on timescales less than ~ 100 s for poloidal fields greater than $\sim 10^{12}$ G. Shear viscosity also redistributes angular momentum. However, molecular viscosity in neutron star matter operates on a typical timescale of $\sim 10^9$ s in a star of $\sim 10^9$ K, so it alone is much less effective in bringing the star into uniform rotation than magnetic braking, unless the initial magnetic field is particularly weak. Turbulent viscosity, if it arises, can act more quickly.

To track the evolution of differential rotation and follow the competition between magnetic braking and viscous damping, we model a spinning star as an infinite, axisymmetric cylinder. We take the gas interior to the star to be homogeneous in density and incompressible, which is a crude but not unreasonable approximation for a neutron star governed by a stiff nuclear equation of state. We adopt cylindrical coordinates (r, ϕ, z) , with the z -axis aligned with the rotation axis of the star. We take the magnetic field to have components only in the r and ϕ directions. We consider two cases: one in which the exterior region of the star is pure vacuum and another in which it is a diffuse plasma at a constant density. We treat the fluid everywhere to be perfectly conducting and allow for the presence of shear viscosity, which we take to be constant.

A similar geometry was adopted previously to study mag-

netic braking of a rotating, cylindrical gas cloud immersed in the interstellar medium (Mouschovias & Paleologou 1979). However, in that analysis it proved sufficient to evolve the magnetic field only in the exterior, treating the cloud as a rigid rotator and ignoring viscosity altogether. Here we are specifically interested in the evolution of the field inside the star and learning exactly how the field and viscosity combine to alter the interior angular momentum profile of a differentially rotating configuration.

3. BASIC EQUATIONS

The fundamental equations for our incompressible, perfectly conducting MHD fluid are the equation of continuity

$$\nabla \cdot \mathbf{v} = 0, \quad (1)$$

where \mathbf{v} is the velocity, and the magnetic Navier-Stokes equation

$$\begin{aligned} \frac{\partial \mathbf{v}}{\partial t} + (\mathbf{v} \cdot \nabla) \mathbf{v} = & \\ - \frac{1}{\rho} \nabla P - \nabla \Phi + \nu \nabla^2 \mathbf{v} + \frac{(\nabla \times \mathbf{B}) \times \mathbf{B}}{4\pi\rho}, & \end{aligned} \quad (2)$$

where ρ is the density, ν is the viscosity, P is the pressure, \mathbf{B} is the magnetic field and Φ is the Newtonian gravitational potential, which satisfies Poisson's equation,

$$\nabla^2 \Phi = 4\pi\rho. \quad (3)$$

The magnetic field \mathbf{B} satisfies Maxwell's constraint equation

$$\nabla \cdot \mathbf{B} = 0, \quad (4)$$

as well as the flux-freezing equation

$$\frac{\partial \mathbf{B}}{\partial t} = \nabla \times (\mathbf{v} \times \mathbf{B}). \quad (5)$$

Solving equation (1) for our cylindrical star gives the radial component of the velocity as $v_r = Rv_0(t)/r$ where R is the stellar radius. Demanding the flow be regular at the origin requires that the function $v_0(t)$ vanish identically, implying that only rotational motion can take place, with an azimuthal velocity given by $v_\phi = r\Omega(t, r)$. Here Ω is the angular velocity. Solving equation (4) for the magnetic field together with the flux-freezing condition (5) requires that the radial component of the magnetic field be independent of time and given by

$$B_r = \frac{B_0 R}{r}, \quad t \geq 0, \quad (6)$$

where B_0 is the value of the field at the stellar surface at $t = 0$. Although the magnetic field given by equation (6) exhibits a static line singularity along the axis at $r = 0$, it does not drive singular behavior in the fluid velocity or nonradial magnetic field. As these quantities, which are the main focus here, remain finite and evolve in a physically reasonable fashion, the line singularity poses no difficulty and requires no special treatment.

Evaluating the azimuthal components of equations (2) and (5), the system then reduces to two coupled partial differential equations for Ω and B_ϕ ,

$$\frac{\partial \Omega}{\partial t} = \frac{RB_0}{4\pi\rho r^3} \frac{\partial}{\partial r} (rB_\phi) + \frac{\nu}{r^3} \frac{\partial}{\partial r} \left(r^3 \frac{\partial \Omega}{\partial r} \right), \quad (7)$$

and

$$\frac{\partial B_\phi}{\partial t} = B_0 R \frac{\partial \Omega}{\partial r}. \quad (8)$$

Equations (7) and (8) are the main dynamical equations to be solved. Once Ω and B_ϕ are determined, the radial component of the Navier- Stokes equation,

$$\frac{\partial P}{\partial r} = \rho \frac{v_\phi^2}{r} - \rho \frac{\partial \Phi}{\partial r} - \frac{1}{4\pi} \left(\frac{1}{2} \frac{\partial B_\phi^2}{\partial r} + \frac{B_\phi^2}{r} \right), \quad (9)$$

can be solved for the pressure as a function of r and t by a simple integration over r . Though straightforward, obtaining the resulting pressure, which is the profile necessary to enforce hydrostatic equilibrium in the star in the radial direction at all times, is not required to obtain the evolution of the rotation profile or magnetic field and is therefore of little interest here. Similarly, the equation of heat transfer is not needed in solving the problem of incompressible flow, as we are not interested here in the temperature distribution.

3.1. Initial Conditions and Boundary Values

We assume that no azimuthal component of the field B_ϕ is present initially,

$$B_\phi(0, r) = 0, \quad r \geq 0, \quad (10)$$

recalling that B_r is always given by equation (6). We are thus interested in the situation where the azimuthal field is created entirely by the differential rotation of the fluid, which bends the frozen-in, initially pure radial field lines in the azimuthal direction.

We solve equation (7) for Ω subject to the condition of regularity at the origin,

$$\frac{\partial \Omega(t, 0)}{\partial r} = 0, \quad t \geq 0, \quad (11)$$

which, by equations (8) and (10), implies

$$\frac{\partial B_\phi(t, 0)}{\partial t} = 0 = B_\phi(t, 0), \quad t \geq 0. \quad (12)$$

The boundary conditions at the stellar surface depend on the physical situation being investigated. In the case of an exterior vacuum, no azimuthal magnetic field can be carried into the region outside the star. This fact, together with equation (8), implies

$$B_\phi(t, R) = 0 = \frac{\partial \Omega(t, R)}{\partial r}, \quad t \geq 0 \quad (\text{vacuum exterior}). \quad (13)$$

In the case where the exterior region of the star contains a conducting homogeneous fluid at density ρ_{ex} , part of the azimuthal field is transmitted across the stellar surface in the form of an outgoing Alfvén wave, and part is reflected via an ingoing Alfvén wave. We construct an appropriate wave boundary condition accounting for partial transmission and reflection at the interface between the interior star and the exterior plasma according to

$$\frac{\partial B_\phi(t, R)}{\partial t} + \frac{\partial B_\phi(t, R)}{\partial r} v_A \frac{(1 + \mathcal{R})}{(1 - \mathcal{R})} = 0 \quad (\text{plasma exterior}), \quad (14)$$

where \mathcal{R} is the reflection coefficient for the azimuthal field amplitude,

$$\mathcal{R} = \frac{(\rho_{\text{ex}}/\rho)^{1/2} - 1}{(\rho_{\text{ex}}/\rho)^{1/2} + 1}, \quad (15)$$

and $v_A = B_0/(4\pi\rho)^{1/2}$ is the Alfvén speed just inside the stellar surface (see Appendix A). The corresponding boundary condition for Ω is

$$\frac{\partial \Omega(t, R)}{\partial r} + \frac{\partial \Omega(t, R)}{\partial t} \frac{1}{v_A} \frac{(1 + \mathcal{R})}{(1 - \mathcal{R})} = 0 \quad (\text{plasma exterior}). \quad (16)$$

Note that when $\rho_{\text{ex}} = 0$, we have $\mathcal{R} = -1$, so equations (14) and (16) recover the vacuum exterior boundary conditions (13), recalling equation (10). By contrast, when $\rho_{\text{ex}} = \rho$, and the exterior plasma is a smooth continuation of the interior star, we have $\mathcal{R} = 0$, and equations (14) and (16) impose standard outgoing (Alfvén) wave boundary conditions on these transverse field and velocity components.

The entire evolution of the system is driven by differential rotation. We take the initial rotation profile of the star to have the following nonuniform, momentarily stationary form:

$$\Omega(0, r) = \frac{1}{2} \Omega_0 [1 + \cos(\pi r^2/R^2)], \quad 0 \leq r \leq R, \quad (17)$$

where

$$\frac{\partial \Omega(0, r)}{\partial t} = 0, \quad 0 \leq r \leq R. \quad (18)$$

We note that our adopted initial angular velocity profile is consistent with the boundary conditions at the center and surface of the star (see equations (11) and (13)), as required.

3.2. Conserved Energy and Angular Momentum

The MHD equations (7) and (8) admit two nontrivial integrals of the motion, one expressing conservation of energy and the other conservation of angular momentum of the star. Energy conservation is given by the integral

$$E_{\text{rot}}(0) = E_{\text{rot}}(t) + E_{\text{mag}}(t) + E_{\text{vis}}(t) + E_{\text{Poynt}}(t), \quad (19)$$

where $E_{\text{rot}}(t)$ is the rotational kinetic energy of the matter, $E_{\text{mag}}(t)$ is the azimuthal magnetic energy, $E_{\text{vis}}(t)$ is the internal (thermal) energy generated by viscous dissipation and $E_{\text{Poynt}}(t)$ is the energy carried off at the stellar surface by the Poynting vector $\mathbf{S} = \mathbf{cE} \times \mathbf{B}/4\pi$, where $\mathbf{E} = -\mathbf{v} \times \mathbf{B}/c$:

$$E_{\text{rot}}(t) = \int d^3x (\rho \Omega^2(t, r) r^2 / 2), E_{\text{mag}}(t) = \int d^3x (B_\phi^2(t, r) / 8\pi) \\ E_{\text{vis}}(t) = \int_0^t dt \dot{E}_{\text{vis}}(t), E_{\text{Poynt}}(t) = \int_0^t dt \dot{E}_{\text{Poynt}}(t). \quad (20)$$

The rates of viscous dissipation $\dot{E}_{\text{vis}}(t)$ and Poynting energy loss $\dot{E}_{\text{Poynt}}(t)$ appearing in equation (20) are given by

$$\dot{E}_{\text{vis}}(t) = \int d^3x \left[\nu \rho \left(\frac{\partial \Omega}{\partial r} \right)^2 r^2 \right], \quad (21)$$

$$\dot{E}_{\text{Poynt}}(t) = - \left(\frac{B_\phi B_r \Omega R}{4\pi} \right)_{r=R} \mathcal{A}.$$

The volume elements in equations (20) and (22) are evaluated as $d^3x = 2\pi L r dr$, with the volume integration performed throughout the interior of the cylindrical star over a (arbitrary) height L in the z -direction. The Poynting flux is measured at

the surface of this region, whose area is $\mathcal{A} = 2\pi LR$. Dividing all quantities by L then gives energies per unit length.

Conservation of angular momentum is expressed as ²

$$J_{\text{rot}}(0) = J_{\text{rot}}(t) + J_{\text{mag}}(t), \quad (22)$$

where J_{rot} is the rotational angular momentum of the matter and J_{mag} is the integrated torque exerted by the Maxwell stress at the surface,

$$J_{\text{rot}}(t) = \int d^3x (\rho \Omega(t, r) r^2), \quad J_{\text{mag}}(t) = \int_0^t dt \mathcal{N}. \quad (23)$$

The torque \mathcal{N} is given by

$$\mathcal{N} = - \left(\frac{B_r B_\phi R}{4\pi} \right)_{r=R} \mathcal{A}. \quad (24)$$

We note that, consistent with the nonrelativistic MHD approximation, the electric field energy $E^2/8\pi$ is not included in equation (19) and the angular momentum of the electromagnetic field S_ϕ/c^2 is not included in equation (22) (Landau, Lifshitz & Pitaevskii 1984).

The motivation for the monitoring the conservation equations during the evolution is twofold: physically, evaluating the individual terms enables us to track how the initial rotational energy and angular momentum in the fluid are transformed, dissipated and/or transported away; computationally, monitoring how well the conservation equations are satisfied provides a check on the numerical integration scheme.

3.3. Nondimensional Formulation

We introduce nondimensional variables to facilitate the integration and to help identify the scaling behavior of our solution with respect to our arbitrary choices of input parameters. We define nondimensional quantities according to

$$\begin{aligned} \hat{r} &= r/R, \quad \hat{t} = 2t/(R/v_A), \quad \hat{\nu} = 4\nu/(v_A R) \\ \hat{\Omega} &= \Omega/\Omega_0, \quad \hat{B}_\phi = B_\phi / \left((4\pi\rho)^{1/2} (\Omega_0 R) \right) \\ \hat{E} &= E / \left((\pi R^2 L \rho) (\Omega_0^2 R^2 / 2) \right), \quad \hat{J} = J / \left((\pi R^2 L \rho) (\Omega_0 R^2) \right). \end{aligned} \quad (25)$$

We work with nondimensional variables in all subsequent equations, but for simplicity we omit placing carets ($\hat{\cdot}$) on the variables. In nondimensional variables, the coupled evolution equations (7) and (8) become

$$\frac{\partial \Omega}{\partial t} = \frac{1}{r^2} \frac{\partial}{\partial r^2} (r B_\phi) + \nu \frac{\partial}{\partial r^4} \left(r^4 \frac{\partial \Omega}{\partial r^2} \right), \quad (26)$$

and

$$\frac{\partial B_\phi}{\partial t} = r \frac{\partial \Omega}{\partial r^2}. \quad (27)$$

When expressed in nondimensional units, the initial value equations and boundary conditions take on the same appearance as in equations (10) – (18), provided we set $v_A = 1 = R$ whenever these quantities appear. Multiplying equation (26) by $\Omega r^2 dr^2$, integrating over the radius of the star and making use of equation (27) yields energy conservation equation (19),

²In deriving both equations (19) and (22) we have set the viscous surface terms proportional to $\nu d\Omega/dr$ equal to zero, which is appropriate for all of the cases treated below.

where the nondimensional energy variables now appearing in that equation are

$$\begin{aligned} E_{\text{rot}}(t) &= \int_0^1 dr^2 \Omega^2(t, r) r^2, \quad E_{\text{mag}}(t) = \int_0^1 dr^2 B_\phi^2, \quad (28) \\ E_{\text{vis}}(t) &= \nu \int_0^t dt \left[\int_0^1 dr^2 \left(\frac{\partial \Omega}{\partial r^2} \right)^2 r^4 \right], \\ E_{\text{Poynt}}(t) &= -2 \int_0^t dt (B_\phi \Omega)_{r=1}. \end{aligned}$$

Multiplying equation (27) by $r^2 dr^2$ and integrating over the star yields² angular momentum conservation equation (22), where the nondimensional angular momentum terms are given by

$$J_{\text{rot}}(t) = \int_0^1 dr^2 \Omega(t, r) r^2, \quad J_{\text{mag}}(t) = - \int_0^t dt (B_\phi)_{r=1}. \quad (29)$$

The coupled system (26) and (27) is purely hyperbolic in the absence of viscosity and leads to a simple wave equation. The inclusion of viscosity gives the system a mixed hyperbolic-parabolic form, since viscosity contributes diffusive damping to the evolution.

4. SOLUTIONS

We solve the evolution equations for three different cases. In case A, we treat a viscous-free star with a vacuum exterior. In case B, we consider the effect of viscosity. In case C, we again ignore viscosity but assume that the exterior region consists of a perfectly conducting plasma of lower density than the central star. By examining these three cases separately we are able to distinguish the different physical processes by which the rotation profile in the star is altered.

4.1. Case A: $\nu = 0$ with vacuum exterior

Here we treat the simplest case in which the fluid is assumed to have no viscosity and the region exterior to the star is a pure vacuum. Setting $\nu = 0$ we take the partial derivative of equation (26) with respect to time and use equation (27) to eliminate B_ϕ , thereby obtaining a simple wave equation for Ω ,

$$\frac{\partial^2 \Omega}{\partial t^2} = \frac{1}{r^2} \frac{\partial}{\partial r^2} \left(r^2 \frac{\partial \Omega}{\partial r^2} \right). \quad (30)$$

This equation must be solved subject to the boundary conditions (11) and (13)

$$\frac{\partial \Omega(t, 0)}{\partial r} = 0 = \frac{\partial \Omega(t, 1)}{\partial r}, \quad (31)$$

and initial conditions (17) and (18)

$$\Omega(0, r) = \frac{1}{2} [1 + \cos(\pi r^2)], \quad \frac{\partial \Omega(0, r)}{\partial t} = 0 \quad (32)$$

We recognize equation (30) as $\square \Omega = 0$ expressed in cylindrical coordinates, with cylindrical radial coordinate $\xi = r^2$ and no dependence on ϕ or z . In these coordinates, the equation is identical to the one that would arise when determining the amplitude of the oscillations of a circular, axisymmetric drumhead, *unclamped* at the outer edge (see, e.g. Mathews & Walker 1970 for an analysis of a circular drumhead that is *clamped* at the outer edge). We solve the equation analytically by separation of variables, obtaining an expansion over Bessel functions according to

$$\Omega(t, r) = \sum_{n=1}^{\infty} A_n J_0(k_n r^2) \cos(k_n t), \quad (33)$$

where

$$A_n = \frac{2 \int_0^1 dr^2 r^2 J_0(k_n r^2) \Omega(0, r)}{J_0^2(k_n)}, \quad (34)$$

and where $\Omega(0, r)$ is set by equation (32). In the above expansion, the quantities $\{k_n\}, n = 1, 2, \dots$ are the zeroes of the derivative of $J_0(x)$, i.e., they satisfy $dJ_0(k_n)/dx = -J_1(k_n) = 0$ and are tabulated (Abramowitz and Stegun (1972), Table 9.5, p. 409, remembering to add $k_1 = 0$). The azimuthal field is obtained by substituting equation (33) into equation (27), integrating over time and using equation (10) to set the initial value. The result is

$$B_\phi = -r \sum_{n=1}^{\infty} A_n J_1(k_n r^2) \sin(k_n t). \quad (35)$$

We evaluate the coefficients A_n up to $n = 20$ by quadrature and the resulting standing wave solutions for the angular velocity and azimuthal magnetic field are shown in Figs. 1 – 3. In Fig. 1 we track the evolution of the various energies with time and observe how the total conserved energy oscillates between rotational kinetic energy of the fluid and energy of the azimuthal magnetic field. The oscillations proceed forever without any dissipation or energy loss. Angular momentum, which is carried entirely by the fluid, is also strictly conserved. We plot the angular velocity profile at critical phases during an oscillation period ($P = 1.64$) in Fig. 2 and we plot the corresponding azimuthal field (a standing Alfvén wave) in Fig. 3.

The series solutions (33) and (35) converge rapidly: the first few values of A_n are $A_1 = 0.2974$, $A_2 = 0.7192$, $A_3 = -0.0198$ and $A_4 = 0.0044$. We already obtain a reasonable approximation by using the first two coefficients alone, together with the quantities $k_1 = 0$ and $k_2 = 3.8317$, to get

$$\Omega(t, r) \approx 0.2974 + (0.7192) J_0(3.8317 r^2) \cos(3.8317 t), \quad (36)$$

and

$$B_\phi \approx -(0.7192) r J_1(3.8317 r^2) \sin(3.8317 t). \quad (37)$$

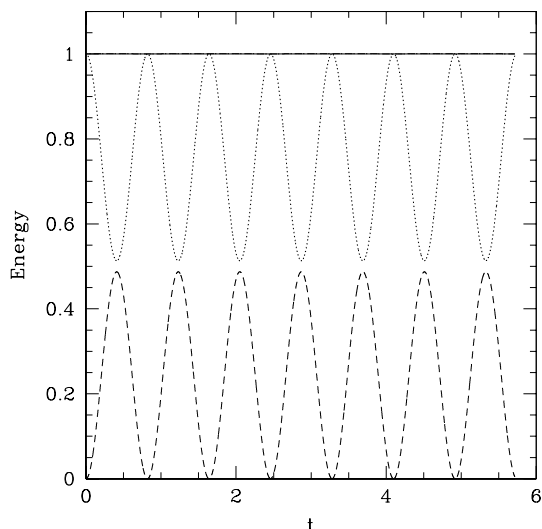


FIG. 1.— Energy evolution for a differentially rotating star with zero viscosity and a vacuum exterior. The dotted line shows E_{rot} and the dashed line shows E_{mag} . All energies are normalized to $E_{\text{rot}}(0)$. The sum of the energies is conserved and remains equal to the initial rotational energy $E_{\text{rot}}(0)$, which is plotted as the solid horizontal line at Energy = 1. Time is in nondimensional units.

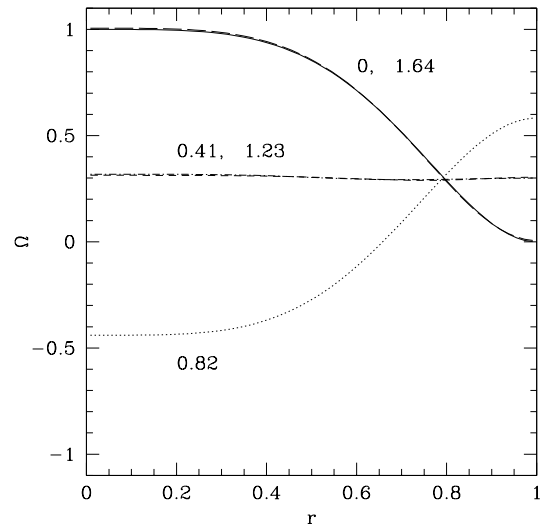


FIG. 2.— The angular velocity profile at critical phases during the first oscillation cycle for the differentially rotating star described in Fig. 1. Curves are labeled by the value of time; the standing wave pattern oscillates with a period $P = 1.64$. All quantities are plotted in nondimensional units.

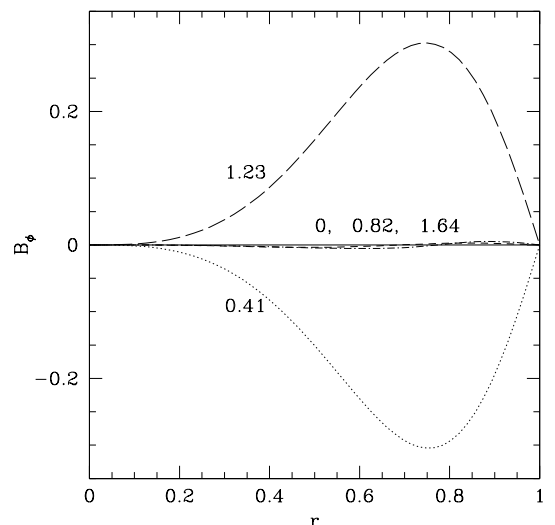


FIG. 3.— The azimuthal magnetic field profile at critical phases during the first oscillation cycle for the differentially rotating star described in Fig. 1. Curves are labeled by the value of time; the standing Alfvén wave pattern repeats with a period $P = 1.64$. All quantities are plotted in nondimensional units.

From the above approximation we derive the oscillation period to be $P \approx 2\pi/k_2 = 1.64$, consistent with the behavior shown in Figs. 1 – 3. From equation (36) we calculate Ω_{unif} , the value of the angular velocity at the phases of uniform rotation, to be $\Omega_{\text{unif}} = A_1 = 0.2974$, consistent with the horizontal lines in Fig. 2. This value of Ω can also be found by invoking angular momentum conservation: setting $J_{\text{rot}}(0)$, the total (initial) angular momentum of our differentially rotating star, obtained using equations (29) and (32), to the angular momentum of a rigidly rotating configuration with the same density profile, we find

$$\Omega_{\text{unif}} = \frac{\pi^2 - 4}{2\pi^2} = 0.2974 \quad (38)$$

At these phases B_ϕ achieves its maximum amplitude. The energy at the uniformly rotating phases is distributed more evenly

between rotational kinetic and azimuthal magnetic field energy. In our model, the rotational energy falls to a fraction $E_{\text{rot}}/E_{\text{rot}}(0) = 2(\pi^2 - 4)^2 / (\pi^2(3\pi^2 - 16)) = 0.513$, while the magnetic energy increases to $E_{\text{mag}}/E_{\text{rot}}(0) = 1 - E_{\text{rot}}/E_{\text{rot}}(0) = 0.487$ at these phases. In the absence of dissipation, the star oscillates about the uniformly rotating state indefinitely.

The presence of internal energy dissipation (e.g., viscosity), however small, will drive a differentially rotating star to a *permanent* state of uniform rotation, since uniform rotation is the lowest energy state at fixed angular momentum (see Appendix B for a proof). In this situation, the dissipated energy ultimately goes into heat, and the azimuthal magnetic field decays away. We will study this behavior in Case B, below. However, even in the absence of dissipation, the presence of a toroidal (here, radial) magnetic field will brake the differential rotation on the time it would take an Alfvén wave, traveling at the local Alfvén speed $v_A(r) = v_A(R)R/r$, to cross the radius of the star. If we define $t_A \equiv R/v_A$, then in the model analyzed here the Alfvén wave crossing time is exactly $t_A/2 = 1$ in nondimensional units.

The scaling behavior of our solution, revealed by our nondimensional formalism, exhibits several significant features. We find that the values of the *amplitudes* of all evolved quantities shown in Figs. 1–3 are entirely independent of the magnitude of the initial radial seed field B_0 given by equation (6). Only the *timescale* of the evolution depends on the strength of the seed field, and it is proportional to the Alfvén time associated with that field. Specifically, no matter what the strength of the initial radial field, the azimuthal magnetic field will grow to the same high value sufficient to brake the differential motion and drive the star to oscillate about the state of uniform rotation. In this state, the energy in the azimuthal field will always grow to make up the difference between the rotational energy in the initial, differentially rotating configuration and the uniformly rotating configuration, independent of the strength of the seed field. By the same token, the evolution timescale is independent of the degree of differential rotation or the rotation period.

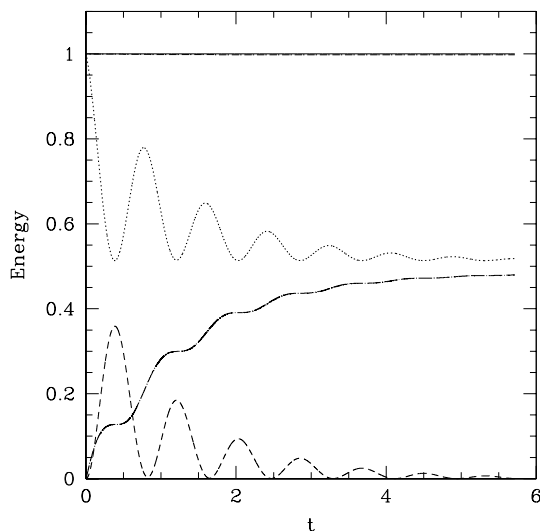


FIG. 4.— Energy evolution for a differentially rotating star with internal viscosity $\nu = 0.2$ and a vacuum exterior. The dotted line shows E_{rot} , the dashed line shows E_{mag} , and the long-dash-dotted line shows E_{vis} . All energies are normalized to $E_{\text{rot}}(0)$. The sum of the energies, plotted as a short-dash-dotted line, is conserved and remains equal to the initial rotational energy $E_{\text{rot}}(0)$, plotted as the solid horizontal line at Energy = 1. Time is in nondimensional units.

4.2. Case B: Nonzero viscosity with vacuum exterior

We now consider the effect of viscous dissipation by setting $\nu = 0.2$ in equation (26). This intermediate value is chosen in order that viscosity in the star be sufficiently large for dissipation to become evident in a few Alfvén timescales, but sufficiently small so that viscous damping of differential rotation does not completely suppress the growth of the azimuthal magnetic field. We solve the coupled evolution equations (26) and (27), subject to the same vacuum exterior boundary and initial conditions used in Case A: equations (10)–(13) for B_ϕ , together with (31) and (32)) for Ω . We solve these equations numerically by finite-differencing (see Appendix C). To better treat the multiple timescales (e.g., Alfvén vs. viscous) and to follow the long-term damping, we employ an implicit scheme and thereby eliminate a Courant stability bound on our numerical timestep. We test our numerical integrations by reproducing the analytic solution derived in Case A for $\nu = 0$ and by checking that energy and angular momentum are conserved according to equations (19) and (22).

The results of our numerical integrations are summarized in Figs. 4–6. In Fig. 4 we track the evolution of the various energies with time. We observe how the oscillations of the rotational kinetic and azimuthal magnetic field energies are now damped by viscosity. From the evolution equation (26), we may define the characteristic viscous dissipation timescale according to $t_\nu = \nu^{-1}$ in nondimensional units, which is equivalent to $t_\nu = R^2/(8\nu)$ in physical units (see equation (25)). For the example considered here, the ratio of viscous to Alfvén time is $t_\nu/t_A = 1/(2\nu) = 2.5$. The numerical results are consistent with this ratio.

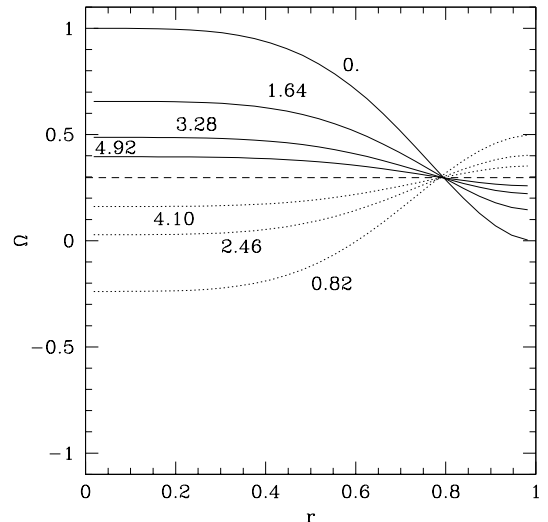


FIG. 5.— The angular velocity profile at critical phases during the first three oscillation cycles for the differentially rotating star described in Fig. 4. Curves are labeled by the value of time. The wave pattern undergoes damped oscillations with a period $P = 1.64$. All quantities are plotted in nondimensional units.

As time progresses, the rotation becomes uniform (see Fig. 5),

the azimuthal field decays back to zero (see Fig. 6), and the rotational energy difference between the initial differentially rotating and the final uniformly rotating star is dissipated as internal heat by the viscosity. Angular momentum is again conserved in the star, as verified by the numerical results. Fig. 4

shows that at late times the final rotational energy approaches $E_{\text{rot}}/E_{\text{rot}}(0) = 0.513$, the value already calculated in Case A for uniform rotation for the given (conserved) angular momentum of our star. At the same time, the energy in viscous dissipation increases to $E_{\text{vis}}/E_{\text{rot}}(0) = 1 - E_{\text{rot}}/E_{\text{rot}}(0) = 0.487$. Similarly, Fig. 5 shows that Ω undergoes damped oscillations about the asymptotic, uniform value Ω_{unif} given by equation (38).

The asymptotic stationary state of the star, which consists of uniform rotation, zero azimuthal magnetic field, and appreciable internal heat content is uniquely determined by conservation of total energy and angular momentum: it does not depend on the strength of the assumed viscosity, only that some viscosity is present, however small. The magnitude of the viscosity does determine the damping timescale for differential rotation and Alfvén wave oscillations. For a sufficiently high viscosity $\nu \gg 1$, differential rotation is damped without driving Alfvén waves throughout the star. However, the final state is unchanged.

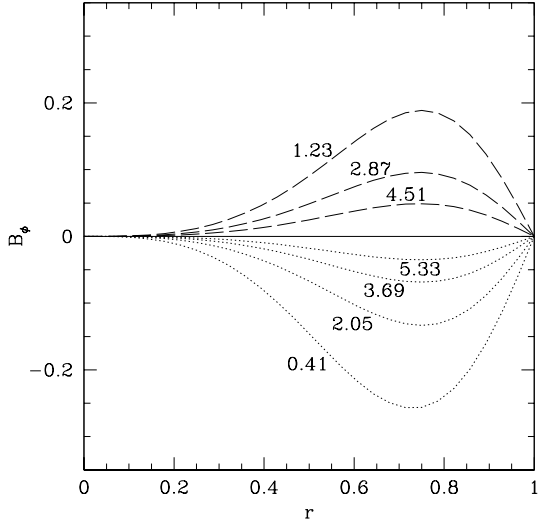


FIG. 6.— The azimuthal magnetic field profile at critical phases during the first three oscillation cycles for the differentially rotating star described in Fig. 4. Curves are labeled by the value of time. The Alfvén wave pattern undergoes damped oscillations with a period $P = 1.64$. All quantities are plotted in nondimensional units.

4.3. Case C: $\nu = 0$ with plasma exterior

Here we treat a differentially rotating star that has no viscosity but is surrounded by an infinite, homogeneous medium of perfectly conducting plasma. We solve the coupled evolution equations (26) and (27) for the same boundary and initial conditions as in Case A, except at the surface, where we now use equation (14) in place of (13) to account for the partial transmission and reflection of the Alfvén wave at the star – plasma interface. We set $\rho_{\text{ex}}/\rho = 0.2$. As in Case B, we again solve the equations by finite differencing (see Appendix C).

Our results are summarized in Figs. 7 – 10, where we see how the loss of energy and angular momentum to the exterior via the transmission of toroidal Alfvén waves drives the star to a slower, rigidly rotating state. In Fig. 7 we observe how the oscillatory exchange of energy between rotation and toroidal magnetic field is damped by the outgoing Poynting energy flux at the surface. Fig. 8 shows how the torque exerted on the star by the magnetic field at the surface causes the star to lose angu-

lar momentum to the exterior plasma. Fig. 9 shows that the angular velocity profile becomes increasingly uniform with time and that the star ends up spinning in the *opposite* sense from its rotation at $t = 0$. By the time the star settles into uniform rotation, the interior azimuthal field dies away, as shown in Fig. 10. Figs. 7 and 8 confirm that total energy and angular momentum are conserved, in compliance with equations (19) and (22).

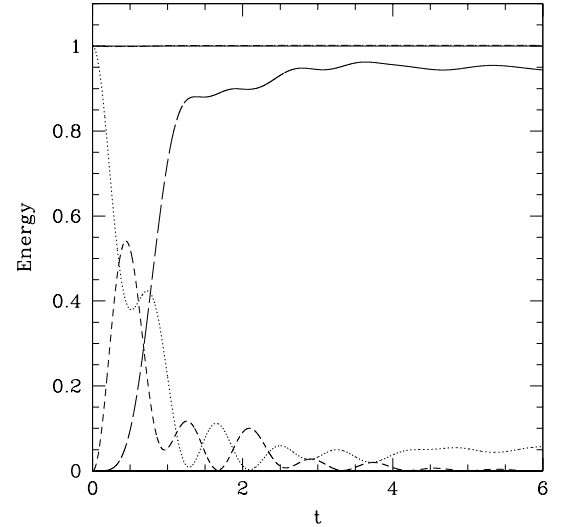


FIG. 7.— Energy evolution for a differentially rotating, zero-viscosity star embedded in an ambient plasma where $\rho_{\text{ex}}/\rho = 0.2$. The dotted line shows E_{rot} , the short-dashed line shows E_{mag} , and the long-dashed line shows the outgoing integrated Poynting energy flux E_{Poynt} . All energies are normalized to $E_{\text{rot}}(0)$. The sum of the energies, indicated by the dot-dashed line, is conserved and remains equal to the initial rotational energy $E_{\text{rot}}(0)$, plotted as the solid horizontal line at Energy = 1. Time is in nondimensional units.

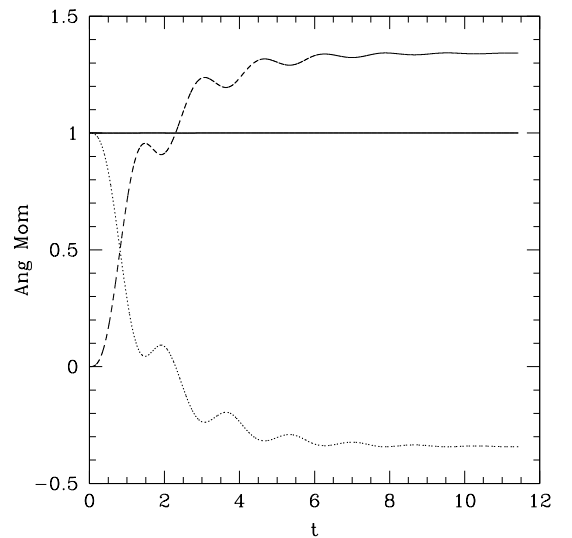


FIG. 8.— Angular momentum evolution for the differentially rotating star depicted in Fig. 7. The dotted curve shows the angular momentum of the star, while the dashed curve shows the integrated torque exerted by the Maxwell stress at the stellar surface. All contributions are normalized to $J_{\text{rot}}(0)$. The sum of all angular momenta, a dot-dashed line, is conserved and remains equal to J_{rot} , plotted as the solid horizontal line at Ang Mom = 1.

The existence of an ambient plasma is sufficient to drive the spin of the star to low values; internal dissipation is not necessary. In this model, the magnitude of the final (retrograde) spin of the star, $\Omega \approx -0.1$, is insensitive to the ratio of the densities of the homogeneous ambient plasma to the homogeneous stellar interior, ρ_{ex}/ρ . This ratio influences the timescale of rotation damping only. A crude estimate suggests that the net damping timescale is roughly $t_{\text{A,ex}} \approx t_{\text{A}}(\rho/\rho_{\text{ex}})^{1/2}$, for small values of ρ_{ex}/ρ . This estimate accounts for the fact that only a fraction $\approx 4(\rho_{\text{ex}}/\rho)^{1/2}$ of the outgoing Poynting energy flux carried by the Alfvén wave actually escapes from the stellar surface into the ambient gas during each oscillation cycle, while the rest is reflected back inward (see equation [A4]).

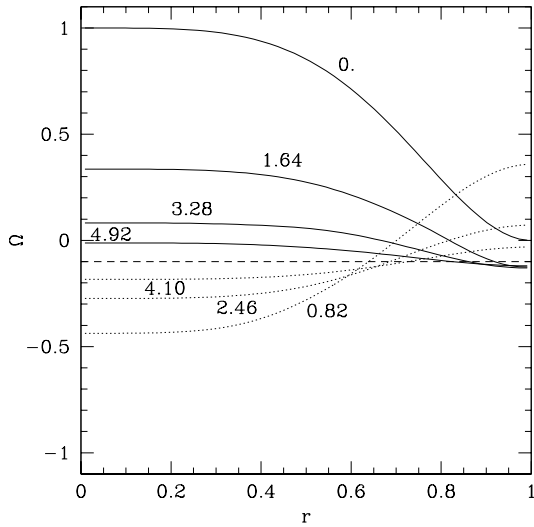


FIG. 9.— The angular velocity profile at critical phases during the first three oscillation cycles for the differentially rotating star described in Fig. 7. Curves are labeled by the value of time. The wave pattern undergoes damped oscillations with a period $P = 1.64$. The star settles into retrograde motion with angular velocity $\Omega \approx -0.1$, indicated by the dashed line. All quantities are plotted in nondimensional units.

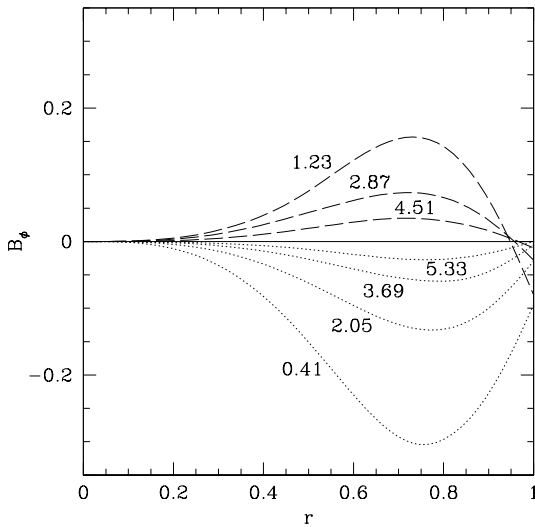


FIG. 10.— The azimuthal magnetic field profile at critical phases during the first three oscillation cycles for the differentially rotating star described in Fig. 7. Curves are labeled by the value of time. The Alfvén wave pattern undergoes damped oscillations with a period $P = 1.64$. All quantities are plotted in nondimensional units.

5. DISCUSSION

The presence of a seed poloidal magnetic field in a differentially rotating star may be sufficient to drive the star to a state of uniform rotation. Differential rotation generates toroidal Alfvén waves through the star and these waves can convert an appreciable fraction of the kinetic energy in differential motion into magnetic field energy. Even in the absence of internal dissipation or Poynting energy loss to an external plasma, the conversion of rotational to magnetic energy by these waves can remove a portion of the star’s rotational support against gravity, which can upset the equilibrium balance in a stationary configuration. In the case of a hypermassive neutron star supported against collapse by differential rotation, the generation of Alfvén waves can lead to catastrophic collapse to a black hole, possibly accompanied by mass loss. Such an outcome may characterize the final fate of neutron stars formed in binary mergers (BSS).

Our model calculations help to identify at least five distinct timescales that govern the evolution of a differentially rotating, equilibrium neutron star containing a seed poloidal magnetic field. We evaluate them here for neutron star parameters consistent with the stable remnant found in the relativistic simulations of binary mergers by Shibata and Uryu (2000). These parameters are comparable to the values of the hypermassive, differentially rotating equilibrium model constructed and evolved by BSS, who found that their configuration was also dynamically stable. All of these models employ a polytropic equation of state with polytropic index $n = 1$, for which there is scale freedom to choose the physical mass. If we take the mass to be $M \approx 2 \times 1.5M_{\odot} \approx 3M_{\odot}$, a reasonable value for a binary remnant, then the equatorial radius of the star is $R \approx 5M \approx 20\text{km}$ and the central angular velocity is $\Omega_0 \approx 0.3/M \approx 2 \times 10^4\text{Hz}$, a factor of three times higher than the angular velocity at the equator.

The dynamical timescale associated with the star is given by

$$t_{\text{dyn}} = \left(\frac{R^3}{M}\right)^{1/2} \approx 0.15 \left(\frac{R}{20\text{km}}\right)^{3/2} \left(\frac{M}{3M_{\odot}}\right)^{-1/2} \text{ ms}, \quad (39)$$

the time it takes the binary remnant to achieve equilibrium following coalescence. This is also the time that it takes the star, once it is driven out-of-equilibrium by magnetic braking, to undergo collapse. The central rotation period of the remnant is

$$t_{\text{rot}} = \frac{2\pi}{\Omega_0} \approx 0.3 \left(\frac{R}{20\text{km}}\right)^{3/2} \left(\frac{M}{3M_{\odot}}\right)^{-1/2} \text{ ms}, \quad (40)$$

while the period at the equator is about three times longer. The timescale for magnetic braking of differential rotation by Alfvén waves is given by

$$t_{\text{A}} = \frac{R}{v_{\text{A}}} \approx 10^2 \left(\frac{B_0}{10^{12}\text{G}}\right)^{-1} \left(\frac{R}{20\text{km}}\right)^{-1/2} \left(\frac{M}{3M_{\odot}}\right)^{1/2} \text{ s}. \quad (41)$$

On this timescale the angular velocity profile in the star is significantly altered, and this change can drive the star far out of equilibrium whenever the initial rotation supplies an appreciable fraction of the support against gravity. In the case of a hypermassive neutron star, which depends on rapid differential rotation for hydrostatic support, magnetic braking can lead to catastrophic collapse to a Kerr black hole, possibly accompanied by some mass and field ejection. A hypermassive star is

a likely outcome of binary neutron star coalescence. The resulting delayed collapse following merger may generate a brief secondary burst of gravitational waves lasting a time t_{dyn} . If the time of the coalescence can be inferred from the initial wave burst signal, then the measurement of this delay should provide an estimate of the strength of the poloidal magnetic field in the interior of the merged neutron star (BSS).

Neutron stars below the supramassive limit do not require differential rotation for hydrostatic support. Such stars have masses at most 20% larger than the nonrotating, spherical TOV limit (see, e.g. Butterworth & Ipson (1975); Friedman, Ipson & Parker (1986); Komatsu, Eriguchi and Hachisu (1989); Cook, Shapiro & Teukolsky 1992,1994; Salgado et al. 1994).³ If such a star is formed with differential rotation, magnetic braking will still drive Alfvén waves in the star and alter the rotation profile on the Alfvén time. While the star may undergo dynamical oscillations, it will not collapse. Instead, viscous dissipation ultimately will drive the star to a new, uniformly rotating equilibrium state on a timescale

$$t_\nu = \frac{R^2}{8\nu} \quad (42)$$

$$\approx 2 \times 10^9 \left(\frac{R}{20\text{km}} \right)^{23/4} \left(\frac{T}{10^9\text{K}} \right)^2 \left(\frac{M}{3M_\odot} \right)^{-5/4} \text{ s},$$

where $\nu = 347\rho^{9/4}T^{-2}\text{cm}^2\text{s}^{-1}$ (Cutler & Lindblom 1987).

If a differentially rotating neutron star is immersed in an ambient plasma at formation, Alfvén waves generated in the interior will propagate into the external medium, carrying off energy and angular momentum. According to equation (A4), everytime a wave propagates to the stellar surface it will transmit a fraction $\approx 4(\rho_{\text{ex}}/\rho)^{1/2}$, ($\rho_{\text{ex}}/\rho \ll 1$), of its energy to the surrounding plasma, causing the star to spindown in an e-folding time

$$t_{\text{A,ex}} = \frac{\ln 2}{4} \left(\frac{\rho}{\rho_{\text{ex}}} \right)^{1/2} t_{\text{A}} \quad (43)$$

$$\approx 20 \left(\frac{B_0}{10^{12}\text{G}} \right)^{-1} \left(\frac{R}{20\text{km}} \right)^{-1/2} \left(\frac{M}{3M_\odot} \right)^{1/2} \left(\frac{\rho}{\rho_{\text{ex}}} \right)^{1/2} \text{ s}.$$

(*cf.* Spitzer 1978, eqn 13.54 and discussion therein for an alternative argument leading to an analogous result). Determining the final spin rate and fate of a newly formed neutron star may thus depend on the nature of its immediate surroundings.

Our naive model calculations do not account for convective instabilities (Pons et al. 1999), which can drive the seed magnetic field to high values greatly exceeding 10^{12}G (Duncan & Thompson 1992), or other possible MHD instabilities, which

may also contribute to the redistribution of angular momentum (Balbus & Hawley 1994; Spruit 1999b). Our main goal was to show that even in the simplest laminar description, a differentially rotating neutron star is a transient phenomenon, since magnetic braking and viscosity inevitably will bring a differentially rotating star into uniform rotation (although not before many dynamical timescales have elapsed, according to our timescale estimates above). Thus all radio pulsars are likely to be uniformly rotating. However, differential rotation may characterize a nascent neutron star formed in a supernova, following fallback, or in a merged binary. The braking of this motion may have important consequences for gravitational wave signals and gamma-ray bursts.

More realistic evolutionary calculations of magnetic braking in neutron stars should clarify some of the above issues. One computational subtlety arises from the inequality $t_{\text{dyn}} \ll t_{\text{A}}$, which holds for seed magnetic fields of small or moderate strength (see equations [39] and [41]). In this regime it may prove too taxing to a relativistic MHD code to evolve a differentially rotating star for the required length of time for magnetic braking to take effect. An obvious solution would be to artificially amplify the initial magnetic field strength, increasing the ratio $t_{\text{dyn}}/t_{\text{A}}$ to a computationally manageable size (while still keeping it much less than unity), and then scale the results for smaller ratios. However, if the energy in the seed magnetic field is an appreciable fraction of the gravitational potential energy, care must be taken to incorporate the magnetic field stresses when constructing the initial hydrostatic equilibrium configuration. Another approach might be to use implicit differencing in the calculation to avoid the Courant stability constraint on the evolution timestep. In addition, one might be able to treat *part* of the evolution in the quasistatic approximation, as in a typical stellar evolution code, up to the moment that stable equilibrium can no longer be sustained. Specifically, one might evolve the magnetic field and the angular velocity on the Alfvén timescale via the MHD equations, but assume hydrostatic equilibrium is maintained on the dynamical timescale in order to determine the density and pressure profiles at each instant. Our idealized incompressible cylindrical star model, which remains radially static, trivially conforms to this behavior and thereby avoids the mismatch between the dynamical and Alfvén timescales. (An additional motivation for treating this idealized problem was to highlight this feature of the analysis.) We hope to tackle the more general problem in future computational investigations.

It is a pleasure to thank T. Baumgarte, C. Gammie and M. Shibata for helpful discussions. This work was supported by NSF Grants AST 96-18524 and NASA Grants NAG 5-7152 and NAG 5-8418 at the University of Illinois at Urbana-Champaign.

APPENDIX

PARTIALLY TRANSMITTED/REFLECTED WAVE OUTER BOUNDARY CONDITION

If the surface of a star is the interface between a highly conducting interior plasma of density ρ and a highly conducting exterior plasma of density ρ_{ex} , an Alfvén wave generated in the interior propagating to the surface suffers partial reflection and transmission (Roberts 1967). The reflection and transmission coefficients for the transverse magnetic field amplitude are

$$\mathcal{R} = \frac{(\rho_{\text{ex}}/\rho)^{1/2} - 1}{(\rho_{\text{ex}}/\rho)^{1/2} + 1} \quad (\text{A1})$$

³The most recent equations of state place the maximum gravitational mass of a spherical star in the range $1.8-2.2M_\odot$ (Akmal, Pandharipande & Ravenhall 1998), but observations of SN 1987A suggest that it could even be as low as $1.5M_\odot$ (Brown & Bethe 1994)

and

$$\mathcal{T} = \frac{2(\rho_{\text{ex}}/\rho)^{1/2}}{(\rho_{\text{ex}}/\rho)^{1/2} + 1} \quad (\text{A2})$$

The reflection and transmission coefficients for the Poynting energy flux are

$$\mathcal{R}_{\text{Poynt}} = \left(\frac{(\rho_{\text{ex}}/\rho)^{1/2} - 1}{(\rho_{\text{ex}}/\rho)^{1/2} + 1} \right)^2 \quad (\text{A3})$$

and

$$\mathcal{T}_{\text{Poynt}} = \frac{4(\rho_{\text{ex}}/\rho)^{1/2}}{((\rho_{\text{ex}}/\rho)^{1/2} + 1)^2}. \quad (\text{A4})$$

Note that $\mathcal{R}_{\text{Poynt}} + \mathcal{T}_{\text{Poynt}} = 1$, in compliance with energy conservation.

We seek to impose an approximate boundary condition on the transverse magnetic field just inside the surface. Decomposing the wave amplitude of the field into its outgoing incident and ingoing reflected components, we may write

$$B_\phi(t, r) = f(t - r/v_A) + \mathcal{R}f(t + r/v_A) \quad (\text{A5})$$

where v_A is the Alfvén propagation speed at the surface. In writing equation (A5) we approximate the wave to be planar, which is strictly true only for wavelengths $\lambda_A \ll R$. Differentiating equation (A5) yields

$$f' = \frac{\partial B_\phi}{\partial t} \frac{1}{(1 + \mathcal{R})} = -\frac{\partial B_\phi}{\partial r} \frac{v_A}{(1 - \mathcal{R})} \quad (\text{A6})$$

where the prime denotes a total derivative. We may then recast equation (A6) as

$$\frac{\partial B_\phi(t, R)}{\partial t} + \frac{\partial B_\phi(t, R)}{\partial r} v_A \frac{(1 + \mathcal{R})}{(1 - \mathcal{R})} = 0, \quad (\text{A7})$$

which provides the desired boundary condition.

UNIFORM ROTATION AS THE LOWEST ENERGY CONFIGURATION

Here we prove that for fixed angular momentum, the angular velocity profile that gives a stationary star of lowest energy is one of uniform rotation. To find the lowest energy state, set the azimuthal magnetic field energy to zero and take the total energy of the configuration to be rotational kinetic energy,

$$E = \int_0^1 dr^2 E(\Omega, r^2) = \int_0^1 dr^2 \Omega^2 r^2, \quad (\text{B1})$$

The conserved angular momentum is given by

$$J = \int_0^1 dr^2 J(\Omega, r^2) = \int_0^1 dr^2 \Omega r^2. \quad (\text{B2})$$

The lowest energy configuration is found by varying the energy subject to the constraint of fixed angular momentum, i.e., by varying the integral

$$\mathcal{I} = E + \lambda J \quad (\text{B3})$$

where λ is a (constant) Lagrange multiplier. Setting the variation equal to zero yields the Euler-Lagrange equation for the functional

$$\mathcal{L}(\Omega, \Omega', r^2) = E(\Omega, r^2) + \lambda J(\Omega, r^2). \quad (\text{B4})$$

The Euler-Lagrange equation gives

$$\frac{d\mathcal{L}}{d\Omega} = (2\Omega + \lambda)r^2 = 0, \quad (\text{B5})$$

or

$$\Omega = -\frac{\lambda}{2} = \text{constant}, \quad (\text{B6})$$

which is the desired result.

FINITE DIFFERENCE EQUATIONS

To finite difference the coupled evolution equations (26) and (27) we introduce a uniform radial grid r_i , $i = 1, 2, \dots, i_{max}$, which extends from $r_1 = 0$ to $r_{i_{max}} = 1$. The angular velocity Ω is defined at the midpoints of the radial zones while the magnetic field B is defined on the zone boundaries. We adopt an implicit evolution scheme in which the differencing is first order in time but second order in space. Care is taken when finite differencing the radial gradients so that they reflect the correct regularity behavior at the origin, where $B \sim a_1 r$, while $\Omega \sim a_0 + a_2 r^2$; here a_0 , a_1 and a_2 are constants.

To evolve Ω for a timestep $\Delta t = t_{n+1} - t_n$ we difference equation (26) according to

$$\frac{\Omega_{i+1/2}^{n+1} - \Omega_{i+1/2}^n}{\Delta t} = \frac{1}{r_{i+1/2}^2} \frac{(r_{i+1} B_{i+1}^{n+1} - r_i B_i^{n+1})}{(r_{i+1}^2 - r_i^2)} \quad (C1)$$

$$+ \frac{\nu}{r_{i+1}^4 - r_i^4} \left(r_{i+1}^4 \frac{(\Omega_{i+3/2}^{n+1} - \Omega_{i+1/2}^{n+1})}{(r_{i+3/2}^2 - r_{i+1/2}^2)} - r_i^4 \frac{(\Omega_{i+1/2}^{n+1} - \Omega_{i-1/2}^{n+1})}{(r_{i+1/2}^2 - r_{i-1/2}^2)} \right)$$

while to evolve B we difference equation (27) according to

$$\frac{B_i^{n+1} - B_i^n}{\Delta t} = r_i \frac{(\Omega_{i+1/2}^{n+1} - \Omega_{i-1/2}^{n+1})}{(r_{i+1/2}^2 - r_{i-1/2}^2)} \quad (C2)$$

Boundary condition (12) at the origin requires

$$B_1^{n+1} = 0. \quad (C3)$$

The outer boundary condition depends on the nature of the exterior medium:

$$B_{i_{max}}^{n+1} = 0, \quad (\text{vacuum exterior}) \quad (C4)$$

according to equation (13), or

$$B_{i_{max}}^{n+1} = B_{i_{max}}^n - \frac{\Delta t}{2(r_{i_{max}} - r_{i_{max}-1})} \left(\frac{1 + \mathcal{R}}{1 - \mathcal{R}} \right) (B_{i_{max}}^n - B_{i_{max}-1}^n), \quad (\text{plasma exterior}), \quad (C5)$$

according to equation (14). The two prescriptions agree in the case of a vacuum exterior, where $\rho_{ex} = 0$ and $\mathcal{R} = -1$, whereby condition (C5) gives $B_{i_{max}}^{n+1} = B_{i_{max}}^n = \dots = B_{i_{max}}^1 = 0$.

Substituting finite difference equation (C2) into (C1) and using equation (C3) at the inner boundary and equation (C4) or (C5) at the outer boundary yields a single tridiagonal matrix equation for Ω^{n+1} . We invert this tridiagonal matrix at each timestep, after which we use equation (C2) again to get B^{n+1} . Since we use implicit differencing in time, the upper bound on the size of our integration timestep Δt is set by accuracy and not stability criteria.

REFERENCES

- Abramowitz, M., & Stegun, I., 1972, Handbook of Mathematical Functions, (New York: Dover)
- Akmal, A., Pandharipande, V. R., & Ravenhall, D. G., 1998, Phys. Rev. C, 58, 1804
- Balbus, S. A., & Hawley, J. F., 1994, MNRAS, 266, 769.
- Baumgarte, T. W., & Shapiro, S. L., & Shibata, M, 2000, ApJ, 528, L29 (BSS)
- Bildsten, L., & Cutler, C., 1992, ApJ, 400, 175
- Brown, G. E., & Bethe, H. A., 1994, ApJ, 423, 659
- Butterworth, I. M., & Ipser, J. R., 1975, ApJ, 200, L103
- Cook, G. B., Shapiro, S. L., & Teukolsky, S. A., 1992 ApJ, 398, 203
- , 1994, ApJ, 422, 227
- Cutler, C., & Lindblom, L., 1987, ApJ, 314, 234
- Duncan, R. C., & Thompson, C., 1992, ApJ, 392, L9
- Friedman, J. L., Ipser, J. R., & Parker, L., 1986, ApJ, 304, 115
- Kochanek, C. S., 1992, ApJ, 398, 234
- Komatsu, H., Eriguchi, Y., & I. Hachisu, 1989, MNRAS, 237, 355
- Lai, D., Rasio, F. A., & Shapiro, S. L., 1993, ApJ, 88, S205
- Landau, L. D., Lifshitz, E. M., & Pitaevskii, L. P., 1984, Electrodynamics of Continuous Media, (Oxford: Pergamon), p. 227
- Mathews, J., & Walker, R. L., Mathematical Methods of Physics, (Menlo Park: Benjamin/Cummings)
- Mouschovias, T. Ch., & Paleologou, E., 1979, ApJ, 230, 204
- Pons, J. A., Reddy, S., Prakash, M., Lattimer, J. M., & Miralles, J. A., 1999, ApJ, 513, 780
- Rampp, M., Müller, E., & Ruffert, M. 1998, A&A, 332, 969
- Roberts, P. H. 1967, An Introduction to Magnetohydrodynamics (New York: American Elsevier) p. 142
- Rasio, F. A., & Shapiro, S. L., 1992, ApJ, 401, 226
- 1994, ApJ, 432, 242
- 1999, Class. Quant. Grav., 16, R1
- Salgado, M., Bonazzola, S., Gourgoulhon, E., & Hansel, P., 1994, A&A, 291, 155
- Shapiro, S. L., & Teukolsky, S. L., 1983, Black Holes, White Dwarfs, and Neutron Stars (New York: Wiley)
- Shibata, M., Baumgarte, T. W., & Shapiro, S. L., 2000, ApJ, in press (astro-ph/0005378)
- Shibata, M., & Uryu, K., 2000, Phys. Rev. D, 61, 064001
- Spitzer, L. Jr., 1978, Physical Processes in the Interstellar Medium, (New York: Wiley)
- Spruit, H. C., 1999a, A&A, 341, L1
- , 1999b, A&A, 349, 189
- Tassoul, J.-L., 1978, Theory of Rotating Stars (Princeton: Princeton Univ. Press)
- Zwerg, T., & Müller, E., 1997, A&A, 320, 209